Active magneto-optical control of spontaneous emission in graphene

W. J. M. Kort-Kamp,[1,2] B. Amorim,[3,4] G. Bastos,[2] F. A. Pinheiro,[2,5] F. S. S. Rosa,[2] N. M. R. Peres,[4] and C. Farina[2]

[1]*Center for Nonlinear Studies and Theoretical Division, Los Alamos National Laboratory, Los Alamos, New Mexico 87545, USA*

[2]*Instituto de Física, Universidade Federal do Rio de Janeiro, Caixa Postal 68528, Rio de Janeiro 21941-972, Rio de Janeiro, Brazil*

[3]*Instituto de Ciencia de Materiales de Madrid, CSIC, Cantoblanco E28049, Madrid, Spain*

[4]*Department of Physics and Center of Physics, University of Minho, P-4710-057 Braga, Portugal*

[5]*Optoelectronics Research Centre and Centre for Photonic Metamaterials, University of Southampton, Highfield, Southampton SO17 1BJ, United Kingdom*

(Received 8 June 2015; revised manuscript received 21 October 2015; published 13 November 2015)

We investigate the spontaneous emission rate of a two-level quantum emitter near a graphene-coated substrate under the influence of an external magnetic field or strain induced pseudomagnetic field. We demonstrate that the application of the magnetic field can substantially increase or decrease the decay rate. We show that a suppression as large as 99% in the Purcell factor is achieved even for moderate magnetic fields. The emitter's lifetime is a discontinuous function of $|\mathbf{B}|$, which is a direct consequence of the occurrence of discrete Landau levels in graphene. We demonstrate that, in the near-field regime, the magnetic field enables an unprecedented control of the decay pathways into which the photon/polariton can be emitted. Our findings strongly suggest that a magnetic field could act as an efficient agent for on-demand, active control of light-matter interactions in graphene at the quantum level.

DOI: 10.1103/PhysRevB.92.205415 PACS number(s): 78.67.Wj, 42.50.Ct, 78.20.Ls, 81.05.ue

The possibility of tailoring light-matter interactions at a quantum level has been a sought-after goal in optics since the pioneer work of Purcell [1], where it was first shown that the environment can strongly modify the spontaneous emission (SE) rate of a quantum emitter. To achieve such objective, several approaches have been proposed so far. One of them is to investigate SE in different system geometries [2–11]. Advances in nanofabrication techniques have not only allowed the increase of the spectroscopic resolution of molecules in complex environments [12], but have also led to the use of nanometric objects, such as antennas and tips, to modify the lifetime and enhance the fluorescence of single molecules [13–16]. The presence of metamaterials may also strongly affect quantum emitters' radiative processes. For instance, the impact of negative refraction and of the hyperbolic dispersion on the SE has been investigated [17–19]. Also, the influence of cloaking devices on the SE of atoms has been recently addressed [20].

Progress in plasmonics has also allowed for an unprecedented control of light-matter interactions at a quantum level. When the emitter is located near a plasmonic structure it may experience a strong enhancement of the local field. This effect can be exploited in the development of important applications in nanoplasmonics [11,21–24]. However, structures made of noble metals are hardly tunable, which unavoidably limit their application in photonic devices. To circumvent these limitations, graphene has emerged as an alternative plasmonic material due to its extraordinary electronic and optical properties [25–30]. Indeed, graphene hosts extremely confined plasmons, facilitating strong light-matter interactions [27–30]. In addition, the plasmon spectrum in doped graphene is highly tunable through electrical or chemical modification of the charge carrier density. Due to these properties, graphene is a promising material platform for several photonic applications, especially in the THz frequency range [29]. At the quantum level, the spatial confinement of surface plasmons in graphene has been shown to modify the SE rate [31,32]. The electromagnetic (EM) field pattern excited by quantum emitters near a graphene sheet [33] further demonstrates the huge field enhancement due to the excitation of surface plasmons. A graphene sheet has also been shown to mediate sub- and superradiance between two quantum emitters [34]. Recently, the electrical control of the relaxation pathways and SE rate in graphene has been observed [35]. Despite all these advances, the achieved modification in the emitter's decay rate remains modest so far. Most of the proposed schemes consider emitters whose transition frequencies are in the optical/near-infrared range, usually far from graphene's intraband transitions. As a consequence, the effects of graphene on the SE rate are only relevant when the emitter is no more than a few dozen nanometers apart.

Here we propose an alternative mechanism to actively tune the lifetime of a THz quantum emitter near a graphene sheet by exploiting its extraordinary magneto-optical properties. We show that the application of a magnetic field $\mathbf{B}$ allows for an unprecedented control of the SE rate for emitter-graphene distances in the micrometer range. This is in contrast to previous proposals, in which the modification of the SE rate was achieved by electrically or chemically altering graphene's doping level. The fact that we consider a low-frequency emitter enables us to probe the effects of intraband transitions in graphene on the decay rate, which have also been unexplored so far. In summary, our key results are (i) a striking 99% reduction of the emitter SE rate compared to the case where $\mathbf{B} = \mathbf{0}$; (ii) a new distance-scaling law for the decay rate that corrects the typical $1/d^4$ behavior and is valid for a broad range of distances and magnetic fields; (iii) a highly nonmonotonic behavior of the SE rate as a function of $|\mathbf{B}|$, with sharp discontinuities in the regime of low temperatures; and (iv) the possibility of tailoring the decay channels into which the photon can be emitted. These findings can be physically explained in terms of the interplay among the different EM modes and of electronic intraband transitions between discrete Landau levels in graphene.

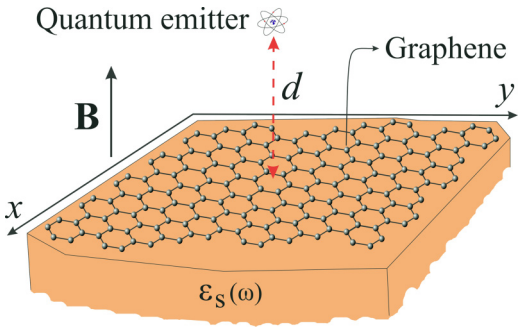

FIG. 1. (Color online) Quantum emitter at a distance d above a graphene sheet on the top of a substrate of permittivity $\varepsilon_s(\omega)$. The whole system is under the influence of a magnetic field $\mathbf{B} = B\hat{\mathbf{z}}$.

I. METHODS

Let us consider the situation depicted in Fig. 1. The half space $z < 0$ is composed of a nonmagnetic, isotropic, and homogeneous material of permittivity $\varepsilon_s(\omega)$, on top of which ($z = 0$) a flat graphene sheet is placed. The system is under influence of a uniform static magnetic field $\mathbf{B} = B\hat{\mathbf{z}}$. The upper medium $z > 0$ is vacuum and an excited quantum emitter is located at a distance d above the interface.

We consider that the quantum emitter dynamics is well described by two of its energy eigenstates ($|g\rangle$ and $|e\rangle$). Within the electric dipole approximation and weak-coupling regime, one can show that the SE rates $\Gamma_\perp$ and $\Gamma_\parallel$ for transition dipole moments perpendicular and parallel to the XY plane, respectively, are (Appendix A) [36–38]

$$\frac{\Gamma_\perp}{\Gamma_0} = 1+\frac{3}{2k_0^3}\,\mathrm{Im}\left\{i\int_0^\infty \frac{k^3 e^{2ik_z d}dk}{k_z} r^{\mathrm{p,p}}\right\}, \quad (1)$$

$$\frac{\Gamma_\parallel}{\Gamma_0} = 1+\frac{3}{4k_0}\,\mathrm{Im}\left\{i\int_0^\infty \frac{k e^{2ik_z d}dk}{k_z}\left[r^{\mathrm{s,s}} - \frac{k_z^2}{k_0^2} r^{\mathrm{p,p}}\right]\right\}, \quad (2)$$

where $\Gamma_0 = |\mathbf{d}_{\mathrm{eg}}|^2\omega_0^3/(3\pi\varepsilon_0\hbar c^3)$ is the free space SE rate, $\mathbf{d}_{\mathrm{eg}}$ is the emitter's electric dipole matrix element, $\omega_0 = k_0 c$ is the transition frequency, $k_z = \sqrt{k_0^2 - k^2}$, and $r^{\mathrm{s,s}}$, $r^{\mathrm{p,p}}$ are the graphene-coated wall polarization-preserving reflection coefficients. Although the cross-polarization reflection coefficients $r^{\mathrm{s,p}}$ and $r^{\mathrm{p,s}}$ are nonvanishing in the case of graphene under the influence of an uniform static magnetic field, being responsible for Faraday and Kerr rotations, they do not contribute to the emitter's lifetime in the present situation (see Appendix A). The diagonal reflection coefficients are given by (Appendix B) [38–40]

$$r^{\mathrm{s,s}} = -\frac{\Lambda^2 + \Delta_+^L\Delta_-^T}{\Lambda^2 + \Delta_+^L\Delta_+^T}, \quad r^{\mathrm{p,p}} = \frac{\Lambda^2 + \Delta_-^L\Delta_+^T}{\Lambda^2 + \Delta_+^L\Delta_+^T}, \quad (3)$$

where $\Lambda^2 = Z_0^2 k_z k_z^s \sigma_H^2$, $\Delta_\pm^L = k_z\varepsilon_s/\varepsilon_0 \pm k_z^s + k_z k_z^s \sigma_L/(\omega\varepsilon_0)$, $\Delta_\pm^T = k_z \pm k_z^s + \mu_0\omega\sigma_T$, $Z_0 = \sqrt{\mu_0/\varepsilon_0}$, $k_z^s = \sqrt{\mu_0\varepsilon_s\omega_0^2 - k^2}$, and $k = |\boldsymbol{k}| = |k_x\hat{\mathbf{x}} + k_y\hat{\mathbf{y}}|$. σ_L, σ_T, and σ_H are the longitudinal, transverse, and Hall conductivities of graphene, respectively, which are, in general, functions of both frequency and transverse wave vector $\boldsymbol{k}$. Although the dependence of the material properties on wave vector may be relevant in the near field [41], we have checked that this is not the case for the distances we consider. Indeed, the evanescent waves contribution to the SE process is suppressed by a e^{-2kd} factor, whereas nonlocal effects on graphene's conductivity become significant for $k \gtrsim \max(\sqrt{eB/\hbar}, \omega_0/v_F, \tau^{-1}/v_F)$ [42,43]. Here $v_F \simeq 10^6$ m/s and τ is a phenomenological relaxation time of electrons in graphene. Therefore, provided $d \gg \min(\sqrt{\hbar/eB}, v_F/\omega_0, v_F\tau)$, we can safely set $k = 0$ in the conductivities, in which case $\sigma_L = \sigma_T$.

We study the lifetime of quantum emitters in the low-temperature ($k_B T \ll \mu_c$) and low-frequency ($\hbar\omega_0 \ll \mu_c$) regimes, where μ_c is the graphene's chemical potential. As a result, graphene's conductivities can be approximated by their intraband terms [29,44–46]

$$\sigma_L = \sigma_T \simeq \sigma_L^{\mathrm{intra}} \simeq \frac{e^3 v_F^2 \hbar B(\omega + i\tau^{-1})(1+\delta_{0,n_c})}{i\pi\,\Delta_{\mathrm{intra}}\left[\Delta_{\mathrm{intra}}^2 - \hbar^2(\omega+i\tau^{-1})^2\right]}, \quad (4)$$

$$\sigma_H \simeq \sigma_H^{\mathrm{intra}} \simeq -\frac{e^3 v_F^2 B(1+\delta_{0,n_c})}{\pi\left[\Delta_{\mathrm{intra}}^2 - \hbar^2(\omega+i\tau^{-1})^2\right]}, \quad (5)$$

where $\Delta_{\mathrm{intra}} = M_{n_c+1} - M_{n_c}$, $M_n = \sqrt{n}M_1$ are the Landau energy levels, $M_1^2 = 2\hbar e B v_F^2$, and $n_c = \mathrm{int}[\mu_c^2/M_1^2]$ denotes the number of occupied Landau levels.

II. RESULTS

Following previous experimental work on SE [47], we consider from now on an emitter with a strong transition at $\omega_0 = 4.2\times10^{12}$ rad/s ($\sim$0.7 THz). We set $\tau = 0.184$ ps [48], $\mu_c = 115$ meV and, inspired by recent experiments on magneto-optical effects in graphene [49], consider a silicon carbide (SiC) substrate. It is important to clarify that ω_0 may be a function of d (the emitter energy levels can be Lamb shifted) and of B (the levels may also be Zeeman shifted). However, for the purposes of the present work, both effects may be neglected. A numerical estimate shows that for the distances considered here, the influence of the Lamb shift on the SE rate is unnoticeable, regardless of the value of B. Concerning the Zeeman shift, we have checked that although some energy levels may be altered in their absolute values, the suppression and enhancement factors of the SE rate due to the application of B are insensitive to this shift.

In Fig. 2 we plot the normalized SE rate $\Gamma_\perp/\Gamma_0$ as a function of the distance d between the emitter and the half space for several values of B. For $d \gtrsim 100\,\mu$m the coupling between the emitter and the graphene-coated wall is mediated by propagating modes ($k \leqslant k_0$) of the vacuum EM field. In this regime of distances the emitter's lifetime is barely affected by B. This behavior results from the fact that in the far field the phase $e^{2ik_z d}$ gives a highly oscillatory integrand in Eq. (1), except for $k_z \sim 0$. In this case, however, $r^{\mathrm{s,s}} \sim r^{\mathrm{p,p}} \sim -1 + \mathcal{O}(k_z/k_0)$, so that the reflectivity of the graphene-coated half space is almost saturated. Hence, B hardly affects the reflection coefficients in this regime. A transition from the oscillating pattern at large distances to a sharp growth at small distances takes place for $d \lesssim 100\,\mu$m. In this regime of distances the emission is dominated by evanescent modes ($k > k_0$) of the vacuum EM field. Interestingly, for $d \lesssim 10\,\mu$m changing B strongly affects the lifetime of the quantum emitter. A striking suppression of

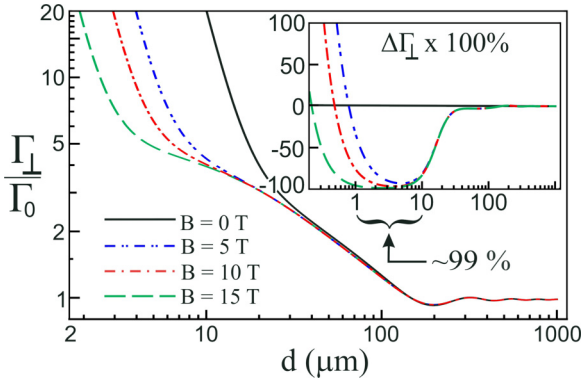

FIG. 2. (Color online) Normalized decay rate $\Gamma_\perp/\Gamma_0$ as a function of distance d between the emitter and the graphene-SiC half space for different magnetic fields. The inset presents the relative SE rate $\Delta\Gamma_\perp$ as a function of d for the same values of B.

99% in the Purcell factor, when compared to the case where $B = 0$ T, occurs for 1 μm $\lesssim d \lesssim$ 10 μm and $B \gtrsim 10$ T. Even for smaller values of B the Purcell effect is greatly reduced. For example, for $d = 3$ μm the influence of the graphene-coated wall on $\Gamma_\perp$ can be reduced by a factor of 10 for $B = 5$ T. These results are highlighted in the inset of Fig. 2, where we plot $\Delta\Gamma_\perp = [\Gamma_\perp(d,B) - \Gamma_\perp(d,0)]/\Gamma_\perp(d,0)$ as a function of d for the same values of B. For even smaller distances an enhancement of the SE rate takes place as the magnetic field increases. For clarity this effect is not shown in Fig. 2, although it can be noticed in the inset for $d \lesssim 1$ μm. For instance, for $B = 5$ T and $d = 0.2$ μm the SE rate is enhanced by ~500%.

It is also interesting to analyze the distance-scaling law of the SE rate for graphene under an external magnetic field. In the near-field regime, one can show that (Appendix C)

$$\frac{\Gamma_\perp}{\Gamma_0} \simeq \frac{3\varepsilon_0 c^3 \mathrm{Re}[\sigma_L]}{\omega_0^4(\varepsilon_s+\varepsilon_0)^2}\frac{1}{d^4}\,F\left[\frac{|\mathrm{Im}\sigma_L|}{\omega_0(\varepsilon_s+\varepsilon_0)d}\right], \qquad (6)$$

where $F(x)$ is defined in Appendix C, provided $\mathrm{Re}[\sigma_L] \ll \omega_0(\varepsilon_s+\varepsilon_0)d$ and $\mathrm{Im}[\varepsilon_s(\omega_0)] \simeq 0$. The validity of this equation is not restricted to the case when a magnetic field is present; rather it is valid whenever correction due to Im σ_L are non-negligible. Equation (6) explains the results in Fig. 2 for a broad range of distances (0.3 μm $\lesssim d \lesssim$ 1.4 μm) and magnetic fields (5 T $\leqslant B \leqslant$ 20 T) with error $\lesssim$10%. The distance scaling law $\Gamma_\perp \propto d^{-4}F(d_0/d)$ [where $d_0 = |\mathrm{Im}\sigma_L|/\omega_0(\varepsilon_s+\varepsilon_0)$] differs from the recently observed result $\Gamma_\perp \propto d^{-4}$, obtained in the case $\mathbf{B} = \mathbf{0}$ [32]. This difference arises due to (low frequency) intraband transitions and losses in graphene, whose signature is coded in the function $F(x)$ appearing in Eq. (6). Indeed, while in the high-frequency regime ($\omega_0 \gg \tau^{-1}$) graphene's conductivity is approximately a real function, this is not true at the frequency considered here ($\omega_0 \sim \tau^{-1}$). However, the $\Gamma_\perp \propto d^{-4}$ can be derived provided $|\mathrm{Im}\ \sigma_L| \ll \omega_0(\varepsilon_s+\varepsilon_0)d$. Since $\mathrm{Im}[\sigma_L]$ is greatly affected by B, the magnetic field could be exploited to tailor the distance ranges where this condition is satisfied, allowing for a real-time control of the distance-scaling law in the near field. Note that the effects of B on the SE are predominantly related to changes in σ_L. We have verified that σ_H can be neglected in Eq. (3) for the chosen material parameters. In this case, the same modifications in the SE rate could be obtained by applying a trigonal distortion to graphene, which would generate a strain induced pseudomagnetic field, giving rise to the formation of Landau levels in graphene's electronic spectrum, while keeping $\sigma_H = 0$ due to time-reversal invariance [50,51].

To understand such an influence of B on the SE rate in the near-field, it is necessary to delve a little deeper into the decay process itself. The spontaneous decay of a source is often associated to the emission of radiation to the far field, but that is not necessarily the case. In particular, in the near-field regime the emitter decays preferentially into nonradiative channels, like surface waves characterized by $k \geqslant \sqrt{\varepsilon_s/\varepsilon_0}k_0$ [52]. For the transition frequency we are considering, $|\mathrm{Re}\ \sigma_L| \sim |\mathrm{Im}\ \sigma_L|$, so that surface magnetoplasmon polaritons [42] are strongly damped, playing essentially no role in the SE process [53]. Nevertheless, the so-called lossy surface waves (LSWs) [41,54,55] are crucial here. These waves correspond to nonradiative processes and emerge in the case where the emitter's energy is transferred directly to the substrate or graphene, generally giving origin to an excitation (e.g., electron-hole pair). Such waves are quickly damped, with their energy being usually converted into heat [41,55]. In the extreme near-field regime, absorption in the materials governs the SE process and the LSWs ($k \gg k_0$) are usually the main channel into which the emitter loses its energy.

In Fig. 3 we unveil the role played by the different decay channels in the emitter's lifetime. Figure 3(a) depicts the decay probabilities $p_\perp^{\mathrm{P}}$, $p_\perp^{\mathrm{TIR}}$, and $p_\perp^{\mathrm{LSW}}$ of energy emission in a propagating (P), totally internal reflected (TIR), or LSW mode, respectively, as functions of d for two different values of B. These probabilities are given by the ratio between the partial decay rates into the aforementioned modes and the total SE rate. The partial contribution of propagating, TIR, and LSW

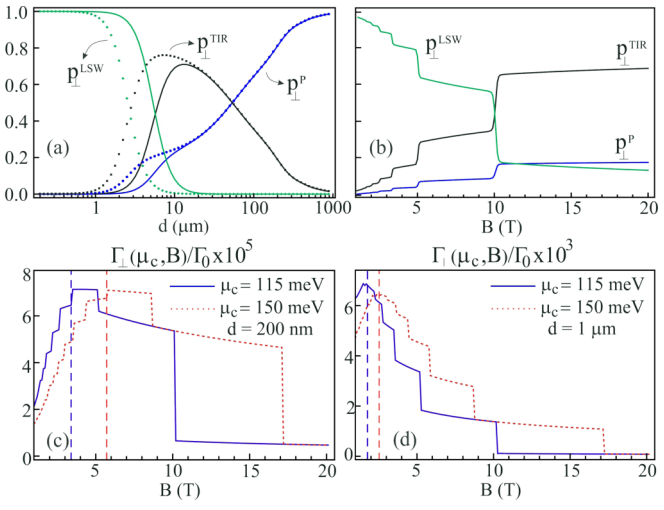

FIG. 3. (Color online) The decay channel probabilities as a function of (a) d and (b) B for $\mu_c = 115$ meV. In (a) solid and dotted curves are for $B = 5$ T and $B = 15$ T, respectively. In (b) the distance is fixed at $d = 4$ μm. $\Gamma_\perp(d,B)/\Gamma_0$ as a function of B is plotted in (c) $d = 200$ nm and (d) $d = 1$ μm. The vertical lines show the position of the peak of $\Gamma_\perp(d,B)/\Gamma_0$ obtained via Eq. (11).

modes to the SE rate can be respectively well approximated by (Appendix D)

$$\frac{\Gamma_\perp^{\rm P}}{\Gamma_0} \simeq 1+\frac{3}{2}\int_0^{k_0} \frac{k^3\,{\rm Re}\left[r^{\rm p,p}e^{2i\sqrt{k_0^2-k^2}d}\right]}{k_0^3\sqrt{k_0^2-k^2}}dk, \tag{7}$$

$$\frac{\Gamma_\perp^{\rm TIR}}{\Gamma_0} \simeq \frac{3}{2}\int_{k_0}^{k_0\sqrt{\frac{\varepsilon_s}{\varepsilon_0}}} \frac{k^3 e^{-2\sqrt{k^2-k_0^2}z}}{k_0^3\sqrt{k^2-k_0^2}}{\rm Im}[r^{\rm p,p}]dk, \tag{8}$$

$$\frac{\Gamma_\perp^{\rm LSW}}{\Gamma_0} \simeq \frac{3}{2}\int_{k_0\sqrt{\frac{\varepsilon_s}{\varepsilon_0}}}^{\infty} \frac{k^2 e^{-2kz}}{k_0^3}{\rm Im}\left[r_{\rm QS}^{\rm p,p}\right]dk, \tag{9}$$

where $r_{\rm QS}^{\rm p,p}$ are the reflection coefficients of the graphene-on-substrate system in the quasistatic limit [equivalent to take $c \to \infty$ in Eq. (3)].

We note in Fig. 3 that changing B can severely affect the possible decay channels in the $1\ \mu{\rm m} \lesssim d \lesssim 10\ \mu{\rm m}$ range, essentially swapping the role of the LSW and TIR modes as the dominant decay pathway. Indeed, for $d = 4\ \mu$m we note that $p_\perp^{\rm LSW}$ drops sharply from 75% to 15% when B changes from 5 to 15 T. On the other hand, $p_\perp^{\rm TIR}$ ($p_\perp^{\rm P}$) increases from 20% (5%) to 67% (18%). This effect is evinced in Fig. 3(b), where we plot the decay probabilities as a function of B, for $d = 4\ \mu$m. It is then clear the overall downward (upward) trend of $p_\perp^{\rm LSW}$ ($p_\perp^{\rm TIR}$) as B is increased, with a dominance exchange at $B \simeq 10$ T.

Figures 3(c) and 3(d) show $\Gamma_\perp(d,B)/\Gamma_0$ as a function of B for $d = 200$ nm and $d = 1\ \mu$m, respectively, and two distinct values of μ_c. The SE rate presents sharp discontinuities, which are directly linked to the discrete character of the Landau levels brought about by the application of $\mathbf{B}$. These discontinuities occur whenever a given Landau level energy crosses μ_c [40,44–46]. Moreover, there exists a critical magnetic field $B_c = \mu_c^2/(2\hbar e v_F^2)$ above which the discontinuities are no longer present. This is due to the fact that for $B > B_c$ all positive Landau levels are above μ_c, so no more crossings can occur. Note that the curves merge in the final plateau, regardless of the value of μ_c. For $B > B_c$ we have $\Delta_{\rm intra} = M_1$, which does not depend on μ_c. Hence, provided $k_BT \ll \mu_c$ both σ_L and σ_H are approximately independent of μ_c for $B > B_c$. As a function of B, the SE rate presents a maximum whose position depends on both μ_c and d. This behavior can be understood recalling that for short distances the SE rate is [32,38]

$$\frac{\Gamma_\perp}{\Gamma_0} \simeq \frac{3}{2k_0^3}\int_0^\infty dk\rho(k){\rm Im}[r^{\rm p,p}(k,\omega_0,B)], \tag{10}$$

where $\rho(k) = k^2e^{-2kd}$ has a maximum at $k_1^{\rm max} = 1/d$. In the large k limit ${\rm Im}[r^{\rm p,p}]$ presents a peak at $k_2^{\rm max} \simeq \varepsilon_0\omega_0[\varepsilon_s/\varepsilon_0 + 1]/|\sigma_L|$. Since $|\sigma_L(\omega_0,B)|$ decreases with B (for $B > 1$ T in our case) we note that $k_2^{\rm max}$ moves to high values of k as B increases. Therefore, for a fixed emitter-graphene separation, the overlap between $\rho(k)$ and ${\rm Im}[r^{\rm p,p}]$ grows with B until $k_2^{\rm max} \sim k_1^{\rm max}$. After that, this overlap diminishes and so does $\Gamma_\perp$, which explains the behavior of the SE rate in Fig. 3. The value of the magnetic field B_m that maximizes $\Gamma_\perp$ can be estimated by setting $k_1^{\rm max} = k_2^{\rm max}$. This leads to

$$|\sigma_L(\omega_0,\mu_c,B_m)| \simeq \varepsilon_0\omega_0 d[\varepsilon_s(\omega_0)/\varepsilon_0 + 1]. \tag{11}$$

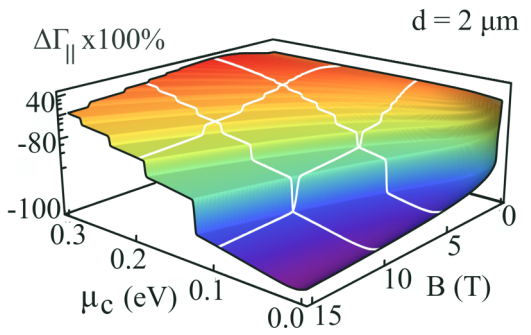

FIG. 4. (Color online) Three-dimensional plot of the relative SE $\Delta\Gamma_\parallel(\mu_c,B)$ as a function of both μ_c and B for $d = 2\ \mu$m.

The accuracy of this equation is clearly seen in Figs. 3(c)–3(d) where we show B_m calculated through Eq. (11) for $\mu_c = 115$ meV and $\mu_c = 150$ meV.

Similar results hold for $\Gamma_\parallel$ in the near-field regime. Indeed, for $d \ll 2\pi/k_0$ the contribution of $r^{\rm s,s}$ to $\Gamma_\parallel$ is negligible and the approximation $k_z \simeq ik$ is valid. Hence, apart from a factor 1/2, $\Gamma_\parallel$ can also be written as in Eq. (10) (see Appendix C) [32]. In Fig. 4 we plot $\Delta\Gamma_\parallel(\mu_c,B) = [\Gamma_\parallel(\mu_c,B) - \Gamma_\parallel(\mu_c,0)]/\Gamma_\parallel(\mu_c,0)$ as a function of both μ_c and B for $d = 2\ \mu$m. In this case, the reduction in the Purcell factor in the μm range can be as high as 98%, when compared to the case $\mathbf{B} = \mathbf{0}$. Figure 4 corroborates our conclusions that an astounding control on the radiative properties of quantum emitters can be achieved via magneto-optical properties in graphene. Moreover, Fig. 4 reveals that the SE rate can be modified by keeping B constant while changing μ_c, which could be implemented by applying a gate voltage on graphene [25–29].

III. CONCLUSION

In conclusion, we have shown that the application of a magnetic field allows for a great control over the Purcell effect and decay pathways of quantum emitters near graphene. Altogether, our findings demonstrate the viability of actively dictating optical energy transfer processes with magnetic fields or strain. By demonstrating that these results are within the reach of state-of-the-art experiments on quantum emission in the THz range, we expect that they may find further applications in quantum photonics and may even serve to probe other light-matter phenomena.

ACKNOWLEDGMENTS

We would like to thank D. A. R. Dalvit, E. C. Marino, F. Guinea, H. Ulbricht, and L. Sapienza for valuable comments. W.J.M.K.-K., G.B., F.S.S.R., and C.F. acknowledge CNPq, CAPES, and FAPERJ for financial support. W.J.M.K.-K. acknowledges financial support from the LANL LDRD program. B.A. acknowledges financial support from Fundação para a Ciência e a Tecnologia, Portugal, through Grant No. SFRH/BD/78987/2011. F.A.P. thanks the Optoelectronics Research Centre and Centre for Photonic Metamaterials, University of Southampton, for the hospitality and CAPES for funding his visit (Grant No. BEX 1497/14-6). F.A.P.

also acknowledges CNPq (Grant No. 303286/2013-0) for financial support. N.M.R.P. acknowledges financial support from the Graphene Flagship Project (Contract No. CNECT-ICT-604391).

APPENDIX A: SPONTANEOUS EMISSION NEAR AN ANISOTROPIC INTERFACE

The SE decay rate of a two-level emitter can be written in terms of the EM dyadic Green's function as

$$\Gamma = \frac{2\omega_0^2}{\varepsilon_0 \hbar c^2} \mathrm{Im}[\mathbf{d}_{\mathrm{ge}}^* \cdot \mathbb{G}(\mathbf{r}_0, \mathbf{r}_0; \omega_0) \cdot \mathbf{d}_{\mathrm{ge}}], \tag{A1}$$

where $\mathbf{r}_0 = (0,0,d)$ is the position of the quantum emitter and $\mathbb{G}(\mathbf{r},\mathbf{r}';\omega)$ is the EM dyadic Green's function, which allows one to write the electric field at position $\mathbf{r}$ that is generated by a point dipole at position $\mathbf{r}'$, oscillating with frequency ω as

$$\mathbf{E}(\mathbf{r};\omega) = \mu\omega^2 \mathbb{G}(\mathbf{r},\mathbf{r}';\omega) \cdot \mathbf{d}(\omega), \tag{A2}$$

where μ is the permeability of the medium where the dipole is embedded. In vacuum the dyadic Green's function satisfies the inhomogeneous Helmholtz equation

$$\boldsymbol{\nabla} \times \boldsymbol{\nabla} \times \mathbb{G}(\mathbf{r},\mathbf{r}';\omega) - \frac{\omega^2}{c^2} \mathbb{G}(\mathbf{r},\mathbf{r}';\omega) = \mathbb{I}\delta(\mathbf{r}-\mathbf{r}'), \tag{A3}$$

with $\mathbb{I}$ being the unit dyad.

We are interested in the case where the emitter is located at a distance d above a semi-infinite homogeneous medium with flat surface at $z = 0$, where the graphene layer lies. Since the dyadic Green's function obeys the same boundary conditions as the electric field, we can write it for $z,z' > 0$ as

$$\mathbb{G}(\mathbf{r},\mathbf{r}';\omega_0) = \mathbb{G}^{(0)}(\mathbf{r},\mathbf{r}';\omega_0) + \mathbb{G}^{(\mathrm{r})}(\mathbf{r},\mathbf{r}';\omega_0), \tag{A4}$$

where $\mathbb{G}^{(0)}(\mathbf{r},\mathbf{r}';\omega_0)$ is the free space Green's function and $\mathbb{G}^{(\mathrm{r})}(\mathbf{r},\mathbf{r}';\omega_0)$ is the reflected one. For $z' > 0$ and $z < 0$, the dyadic Green's function can be written as a transmitted Green's function, $\mathbb{G}^{(\mathrm{t})}(\mathbf{r},\mathbf{r}';\omega_0)$. Each of these Green's functions can be conveniently expressed in terms of its spatial two-dimensional Fourier transform $\tilde{\mathbb{G}}^{(0/\mathrm{r}/\mathrm{t})}(\boldsymbol{k},z,z';\omega)$ as [36]

$$\mathbb{G}^{(0/\mathrm{r}/\mathrm{t})}(\mathbf{r},\mathbf{r}';\omega) = \int \frac{d^2\boldsymbol{k}}{(2\pi)^2} e^{i\boldsymbol{k}\cdot(\boldsymbol{x}-\boldsymbol{x}')} \tilde{\mathbb{G}}^{(0/\mathrm{r}/\mathrm{t})}(\boldsymbol{k},z,z';\omega), \tag{A5}$$

where $\boldsymbol{k} = k_x\hat{\mathbf{x}} + k_y\hat{\mathbf{y}}$ and $\boldsymbol{x} = x\hat{\mathbf{x}} + y\hat{\mathbf{y}}$. The free space Green's function is given by

$$\tilde{\mathbb{G}}^{(0)}(\boldsymbol{k},z,z';\omega) = \frac{i}{2k_z} e^{ik_z|z-z'|} (\boldsymbol{\epsilon}_{\mathrm{p}}^{\pm} \otimes \boldsymbol{\epsilon}_{\mathrm{p}}^{\pm} + \boldsymbol{\epsilon}_{\mathrm{s}}^{\pm} \otimes \boldsymbol{\epsilon}_{\mathrm{s}}^{\pm}), \tag{A6}$$

with k_z defined as

$$k_z = \begin{cases} \sqrt{k_0^2 - k^2}, & k < k_0, \\ i\sqrt{k^2 - k_0^2}, & k > k_0, \end{cases} \tag{A7}$$

and we have introduced the polarization vectors for s- and p-polarized waves (the $+$ and $-$ signs correspond to $z > z'$ and $z < z'$, respectively),

$$\boldsymbol{\epsilon}_{\mathrm{s}}^{\pm} = \frac{k_y\hat{\mathbf{x}} - k_x\hat{\mathbf{y}}}{k}, \qquad \boldsymbol{\epsilon}_{\mathrm{p}}^{\pm} = \frac{k}{k_0}\hat{\mathbf{z}} \mp \frac{k_z}{k_0}\frac{k_x\hat{\mathbf{x}} + k_y\hat{\mathbf{y}}}{k}. \tag{A8}$$

Note that these vectors are orthogonal, but they are normalized only for propagating modes ($k < k_0$).

The reflected Green's function can be written as

$$\tilde{\mathbb{G}}^{(\mathrm{r})}(\boldsymbol{k},z,z';\omega) = \frac{i}{2k_z} e^{ik_z(z+z')} \sum_{\mathrm{i,j=s,p}} r^{\mathrm{i,j}} \boldsymbol{\epsilon}_{\mathrm{i}}^{+} \otimes \boldsymbol{\epsilon}_{\mathrm{j}}^{-}, \tag{A9}$$

where $r^{\mathrm{i,j}}$ are the reflection coefficients for an incoming j-polarized wave that is reflected as an i-polarized wave. Similarly, the transmitted Green's function is given by

$$\tilde{\mathbb{G}}^{(\mathrm{t})}(\boldsymbol{k},z,z';\omega) = \frac{i}{2k_z} e^{-ik_z^s z} e^{ik_z z'} \sum_{\mathrm{i,j=s,p}} t^{\mathrm{i,j}} \boldsymbol{\epsilon}_{\mathrm{i},t}^{-} \otimes \boldsymbol{\epsilon}_{\mathrm{j}}^{-}, \tag{A10}$$

where $t^{\mathrm{i,j}}$ are the transmission coefficients (incoming j-polarized wave, transmitted i-polarized wave) and $\boldsymbol{\epsilon}_{\mathrm{i},t}^{\pm}$ are the polarization vectors in the substrate, given by Eq. (A8) after replacing k_0 by $k_0\sqrt{\varepsilon_s/\varepsilon_0}$ and k_z by k_z^s. The reflection and transmission coefficients are obtained by imposing the usual boundary conditions on the EM field at $z = 0$ and by modeling graphene as a two-dimensional current distribution (see Appendix B).

The evaluation of the SE rate requires the evaluation of the dyadic Green's function at the coincidence $\mathbf{r}' = \mathbf{r} = \mathbf{r}_0$. In this case the integration over the momentum angular variable in Eq. (A5) can be easily performed. The only nonzero components of $\mathbb{G}^{(0)}(\mathbf{r}_0,\mathbf{r}_0;\omega_0)$ are the diagonal ones. The contribution of $\mathbb{G}^{(\mathrm{r})}(\mathbf{r}_0,\mathbf{r}_0;\omega_0)$ to the SE rate presents polarization-preserving terms (which involve $\boldsymbol{\epsilon}_{\mathrm{p}}^{+} \otimes \boldsymbol{\epsilon}_{\mathrm{p}}^{-}$ and $\boldsymbol{\epsilon}_{\mathrm{s}}^{+} \otimes \boldsymbol{\epsilon}_{\mathrm{s}}^{-}$) and cross-polarization terms (which involve $\boldsymbol{\epsilon}_{\mathrm{p}}^{+} \otimes \boldsymbol{\epsilon}_{\mathrm{s}}^{-}$ and $\boldsymbol{\epsilon}_{\mathrm{s}}^{+} \otimes \boldsymbol{\epsilon}_{\mathrm{p}}^{-}$). After performing the angular integration, the polarization-preserving terms only select the diagonal terms of $\mathbf{d}_{\mathrm{ge}}^* \otimes \mathbf{d}_{\mathrm{ge}}$. The cross-polarization terms select the $d_{\mathrm{ge,x}}^* d_{\mathrm{ge,y}} - d_{\mathrm{ge,y}}^* d_{\mathrm{ge,x}}$ components of the dipole matrix elements. As the transition dipole matrix elements of a two-level system can be made real by a proper choice of the relative phase between $|\mathrm{g}\rangle$ and $|\mathrm{e}\rangle$, the cross-polarization terms do not contribute to the SE rate. Therefore, only the reflection coefficients $r^{\mathrm{p,p}}$ and $r^{\mathrm{s,s}}$ give a nonvanishing contribution to the SE process even though cross-polarization coefficients $r^{\mathrm{s,p}}$ and $r^{\mathrm{p,s}}$ are nonzero. Similar conclusions hold even in the case of a semi-infinite anisotropic substrate. By plugging Eqs. (A4)–(A9) into (A1) it is straightforward to obtain Eqs. (1) and (2).

APPENDIX B: FRESNEL'S COEFFICIENTS FOR AN INTERFACE COATED WITH A TWO-DIMENSIONAL CONDUCTIVE FILM IN THE PRESENCE OF AN APPLIED MAGNETIC FIELD

Let us consider that an incoming arbitrarily polarized EM wave propagating in a dielectric medium with permittivity ε_1 and permeability μ_1 impinges on the flat interface with a second homogeneous medium, with permittivity ε_2 and permeability μ_2, occupying the half space $z \leqslant 0$ coated by a two-dimensional (2D) conductive film. For an impinging EM wave with frequency ω and in-plane wave vector $\boldsymbol{k}$, the electric and magnetic fields can be expressed as

$$\mathbf{E}_I = \left[E_I^{\mathrm{s}} \epsilon_{\mathrm{s},1}^{+} + E_I^{\mathrm{p}} \epsilon_{\mathrm{p},1}^{+}\right] e^{-ik_{z,1}z} e^{i(\boldsymbol{k}\cdot\boldsymbol{x}-\omega t)}, \tag{B1}$$

$$\mathbf{H}_I = \frac{1}{Z_1}\left[E_I^{\mathrm{p}} \epsilon_{\mathrm{s},1}^{+} - E_I^{\mathrm{s}} \epsilon_{\mathrm{p},1}^{+}\right] e^{-ik_{z,1}z} e^{i(\boldsymbol{k}\cdot\boldsymbol{x}-\omega t)}, \tag{B2}$$

where $E_I^{\rm s}, E_I^{\rm p}$ are the transverse electric and transverse magnetic incoming amplitudes, respectively. $k_{z,n}$ and $\boldsymbol{\epsilon}^{\pm}_{s/p,n}$ are given by Eqs. (A7) and (A8) replacing k_0 with $k_n = \omega\sqrt{\varepsilon_n\mu_n}$, with $n = 1,2$. $Z_n = \sqrt{\mu_n/\varepsilon_n}$ is the impedance of medium n. Similarly, the reflected and transmitted fields are written as

$$\mathbf{E}_R = \left[E_R^{\rm s}\epsilon^-_{\rm s,1} + E_R^{\rm p}\epsilon^-_{\rm p,1}\right]e^{ik_{z,1}z}e^{i(\boldsymbol{k}\cdot\boldsymbol{x}-\omega t)}, \tag{B3}$$

$$\mathbf{H}_R = \frac{1}{Z_1}\left[E_R^{\rm p}\epsilon^-_{\rm s,1} - E_R^{\rm s}\epsilon^-_{\rm p,1}\right]e^{ik_{z,1}z}e^{i(\boldsymbol{k}\cdot\boldsymbol{x}-\omega t)}, \tag{B4}$$

and

$$\mathbf{E}_T = \left[E_T^{\rm s}\epsilon^+_{\rm s,2} + E_T^{\rm p}\epsilon^+_{\rm p,2}\right]e^{-ik_{z,2}z}e^{i(\boldsymbol{k}\cdot\boldsymbol{x}-\omega t)}, \tag{B5}$$

$$\mathbf{H}_T = \frac{1}{Z_2}\left[E_T^{\rm p}\epsilon^+_{\rm s,2} - E_T^{\rm s}\epsilon^+_{\rm p,2}\right]e^{-ik_{z,2}z}e^{i(\boldsymbol{k}\cdot\boldsymbol{x}-\omega t)}. \tag{B6}$$

We should determine the reflected $E_R^{\rm s(p)}$ and transmitted $E_T^{\rm s(p)}$ amplitudes in order to calculate the reflection and transmission coefficients,

$$r^{\rm i,j} = \frac{E_R^{\rm i}}{E_I^{\rm j}} \quad \text{and} \quad t^{\rm i,j} = \frac{E_T^{\rm i}}{E_I^{\rm j}}, \quad ({\rm i,j}) = ({\rm s,p}). \tag{B7}$$

The reflected and transmitted amplitudes are obtained by solving Maxwell's equations and imposing the appropriate boundary conditions on the interface at $z = 0$. Taking into account the presence of a 2D conductive film at the $z = 0$, the boundary conditions that must be satisfied by the EM field are

$$\hat{\mathbf{z}} \times [\mathbf{E}_T - \mathbf{E}_R - \mathbf{E}_I] = \mathbf{0}, \tag{B8}$$

$$\hat{\mathbf{z}} \times [\mathbf{H}_T - \mathbf{H}_R - \mathbf{H}_I] = \mathbf{J}_{\rm 2D} = \sigma \cdot \mathbf{E}_T, \tag{B9}$$

where $\mathbf{J}_{\rm 2D}$ is a 2D current density that is induced on the conductive field and $\boldsymbol{\sigma}$ is the 2D conductivity tensor of the film [56]. In the most general case (a 2D homogeneous anisotropic material in the presence of a magnetic field) the conductivity tensor can be written as

$$\begin{aligned}\boldsymbol{\sigma} = {}& \sigma_L\hat{\mathbf{e}}_\parallel \otimes \hat{\mathbf{e}}_\parallel + \sigma_T\hat{\mathbf{e}}_\perp \otimes \hat{\mathbf{e}}_\perp \\ & + \sigma_H(\hat{\mathbf{e}}_\perp \otimes \hat{\mathbf{e}}_\parallel - \hat{\mathbf{e}}_\parallel \otimes \hat{\mathbf{e}}_\perp) \\ & + \sigma_{xy}^{\rm sym}(\hat{\mathbf{e}}_\perp \otimes \hat{\mathbf{e}}_\parallel + \hat{\mathbf{e}}_\parallel \otimes \hat{\mathbf{e}}_\perp),\end{aligned} \tag{B10}$$

where $\hat{\mathbf{e}}_\parallel = (k_x\hat{\mathbf{x}} + k_y\hat{\mathbf{y}})/|\boldsymbol{k}|$ and $\hat{\mathbf{e}}_\perp = (k_y\hat{\mathbf{x}} - k_x\hat{\mathbf{y}})/|\boldsymbol{k}|$. σ_L (σ_T) is the longitudinal (transverse) conductivity, σ_H is the Hall conductivity and $\sigma_{xy}^{\rm sym}$ is only nonzero in anisotropic materials such as black phosphorus [57]. In the case of graphene we have $\sigma_{xy}^{\rm sym} = 0$, but, in order to keep the discussion as general as possible and due to the rising interest in black phosphorus, we allow for a finite $\sigma_{xy}^{\rm sym}$. Using Eqs. (B1)–(B6) in Eq. (B8) and Eq. (B9), one can demonstrate that the reflected and transmitted amplitudes satisfy the following equations:

$$E_I^{\rm s} + E_R^{\rm s} = E_T^{\rm s}, \tag{B11}$$

$$\frac{k_{z,1}}{k_1}\left(E_I^{\rm p} - E_R^{\rm p}\right) = \frac{k_{z,2}}{k_2}E_T^{\rm p}, \tag{B12}$$

$$\begin{aligned}\frac{1}{Z_1}\frac{k_{z,1}}{k_1}\left(E_I^{\rm s} - E_R^{\rm s}\right) = {}& \left(\sigma_T + \frac{1}{Z_2}\frac{k_{z,2}}{k_2}\right)E_T^{\rm s} \\ & + \left(\sigma_{xy}^{\rm sym} + \sigma_H\right)\frac{k_{z,2}}{k_2}E_T^{\rm p},\end{aligned} \tag{B13}$$

$$\frac{1}{Z_1}\left(E_I^{\rm p} + E_R^{\rm p}\right) = \left(\sigma_L\frac{k_{z,2}}{k_2} + \frac{1}{Z_2}\right)E_T^{\rm p} + \left(\sigma_{xy}^{\rm sym} - \sigma_H\right)E_T^{\rm s}. \tag{B14}$$

Considering separately the cases of s and p incident polarization, one can decouple previous equations and show that Fresnel's coefficients in the presence of an external magnetic field are given as

$$r^{\rm p,p} = \frac{\Delta_+^T\Delta_-^L + \Lambda^2}{\Delta_+^T\Delta_+^L + \Lambda^2}, \qquad r^{\rm s,s} = -\frac{\Delta_-^T\Delta_+^L + \Lambda^2}{\Delta_+^T\Delta_+^L + \Lambda^2}, \tag{B15}$$

$$t^{\rm p,p} = \frac{Z_2\varepsilon_2}{Z_1\varepsilon_0}\frac{2k_{z,1}\Delta_+^T}{\Delta_+^T\Delta_+^L + \Lambda^2}, \quad t^{\rm s,s} = \frac{\mu_2}{\mu_0}\frac{2k_{z,1}\Delta_+^L}{\Delta_+^T\Delta_+^L + \Lambda^2}, \tag{B16}$$

$$r^{\rm s,p} = t^{\rm s,p} = -2\frac{Z_0^2}{Z_1}\frac{\mu_1\mu_2}{\mu_0^2}\frac{k_{z,1}k_{z,2}\left(\sigma_{xy}^{\rm sym} + \sigma_H\right)}{\Delta_+^T\Delta_+^L + \Lambda^2}, \tag{B17}$$

$$r^{\rm p,s} = -\frac{k_1k_{z,2}}{k_2k_{z,1}}\,t^{\rm p,s} = 2\frac{Z_0^2}{Z_1}\frac{\mu_1\mu_2}{\mu_0^2}\frac{k_{z,1}k_{z,2}\left(\sigma_{xy}^{\rm sym} - \sigma_H\right)}{\Delta_+^T\Delta_+^L + \Lambda^2}, \tag{B18}$$

with

$$\Delta_\pm^L = (k_{z,1}\varepsilon_2 \pm k_{z,2}\varepsilon_1 + k_{z,1}k_{z,2}\sigma_L/\omega)/\varepsilon_0, \tag{B19}$$

$$\Delta_\pm^T = (k_{z,2}\mu_1 \pm k_{z,1}\mu_2 + \omega\mu_1\mu_2\sigma_T)/\mu_0, \tag{B20}$$

$$\Lambda^2 = Z_0^2\mu_1\mu_2k_{z,1}k_{z,2}\left[\sigma_H^2 - (\sigma_{xy}^{\rm sym})^2\right]/\mu_0^2. \tag{B21}$$

For graphene $\sigma_{xy}^{\rm sym} = 0$ and, in the case where medium 1 is vacuum ($\varepsilon_1 = \varepsilon_0$, $\mu_1 = \mu_0$) and medium 2 is nonmagnetic ($\mu_2 = \mu_0$), the reflection coefficients reduce to the ones given in the main text, Eq. (3).

APPENDIX C: DISTANCE-SCALING LAW IN THE NEAR FIELD FOR TERAHERTZ EMITTERS

In the near field, the main contribution for the SE rate in Eqs. (1) and (2) comes from large in-plane wave vectors $k \gg k_0$. In this case the quasistatic approximation holds ($c \to \infty$) and k_z and k_z^s can be well approximated by ik. Besides, the Hall conductivity gives a negligible contribution to the quasistatic reflection coefficients so that we can set $\sigma_H \simeq 0$. Within these approximations the dominant terms in $\Gamma_\perp$ and $\Gamma_\parallel$ originate from the polarization-preserving transverse magnetic reflection coefficient and can be cast as

$$\frac{\Gamma_\perp}{\Gamma_0} \simeq \frac{3}{2}\int_0^{+\infty} dk\,\frac{k^2}{k_0^3}e^{-2kd}\,{\rm Im}\left[r_{\rm QS}^{\rm p,p}\right], \tag{C1}$$

$$\frac{\Gamma_\parallel}{\Gamma_0} \simeq \frac{3}{4}\int_0^{+\infty} dk\,\frac{k^2}{k_0^3}e^{-2kd}\,{\rm Im}\left[r_{\rm QS}^{\rm p,p}\right], \tag{C2}$$

where

$$r_{\rm QS}^{\rm p,p} = \frac{i(\varepsilon_s - \varepsilon_0)\omega_0 - k\sigma_L}{i(\varepsilon_0 + \varepsilon_s)\omega_0 - k\sigma_L}. \tag{C3}$$

In a regime where $|{\rm Re}[\sigma_L]| \ll (\varepsilon_0 + \varepsilon_s)\omega_0 d$ the imaginary part of $r_{\rm QS}^{\rm p,p}$ can be approximated by

$${\rm Im}\left[r_{\rm QS}^{\rm p,p}\right] \simeq \frac{2\varepsilon_0\omega_0k{\rm Re}[\sigma_L]}{\{(\varepsilon_s + \varepsilon_0)\omega_0 - k{\rm Im}[\sigma_L]\}^2}. \tag{C4}$$

Substituting Eq. (C4) into Eqs. (C1) and (C2) one can show that the Purcell factor in the near-field regime is given by

$$\frac{\Gamma_\perp}{\Gamma_0} \simeq \frac{3\varepsilon_0 c^3 \mathrm{Re}[\sigma_L]}{(\varepsilon_0+\varepsilon_s)^2\omega_0^4}\frac{1}{d^4}\,F\left\{\frac{|\mathrm{Im}[\sigma_L]|}{(\varepsilon_0+\varepsilon_s)\omega_0 d}\right\}, \tag{C5}$$

$$\frac{\Gamma_\parallel}{\Gamma_0} \simeq \frac{3\varepsilon_0 c^3 \mathrm{Re}[\sigma_L]}{2(\varepsilon_0+\varepsilon_s)^2\omega_0^4}\frac{1}{d^4}\,F\left\{\frac{|\mathrm{Im}[\sigma_L]|}{(\varepsilon_0+\varepsilon_s)\omega_0 d}\right\}, \tag{C6}$$

with the function $F(x)$ defined as

$$F(x) = \int_0^{+\infty} dy \frac{y^3 e^{-2y}}{(1+yx)^2}. \tag{C7}$$

APPENDIX D: DECAY CHANNEL PROBABILITIES

In order to determine the different decay pathways probabilities, one must study how the total power emitted is distributed into the different channels. Two processes can be distinguished: (i) radiative decay, which involves the emission of a photon that can be detected by a far away detector; (ii) nonradiative decay, where the emitted power does not reach the far field, but is instead absorbed by graphene or substrate and creates a material excitation. In order to compute each channel contribution to the decay process, we use the fact that the total SE rate given by Eq. (A1) corresponds also to the power emitted by a classical oscillating dipole, $\mathbf{d}(t) = \mathbf{d}e^{-i\omega_0 t} + \mathbf{d}^* e^{i\omega_0 t}$. The classical power emitted by such dipole is related to the SE rate of a two-level quantum emitter through $P = \hbar\omega_0\Gamma$ [36,37], provided we choose for $\mathbf{d}$ the transition dipole moment of the quantum emitter. The probability of decaying into a radiative or nonradiative channel can be obtained by computing the fraction of the power that is emitted by the classical dipole to the far field and the one that is dissipated into the materials, respectively.

The average power emitted by the classical dipole that reaches the far field (radiative processes) can be expressed as

$$P_{\mathrm{rad}} = \lim_{r\to\infty}\int_0^{2\pi} d\phi \int_0^{\pi} d\theta\, \sin(\theta)\, r^2 \hat{\mathbf{r}}\cdot\langle\mathbf{S}(\mathbf{r})\rangle, \tag{D1}$$

where the Poynting vector in the far field is given by

$$\mathbf{S}(\mathbf{r},t) = \frac{1}{Z}\mathbf{E}(\mathbf{r},t)\cdot\mathbf{E}(\mathbf{r},t)\hat{\mathbf{r}}, \tag{D2}$$

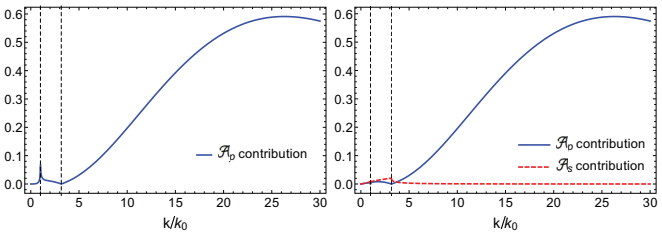

FIG. 5. (Color online) Integrands of Eqs. (D10) and (D11) for the quantum emitter's dissipated power by nonradiative processes. On the left we plot the the integrand of Eq. (D10); on the right we plot the integrand of (D11), splitting it into the individual contributions from the absorption coefficients $\mathcal{A}_\mathrm{p}$ and $\mathcal{A}_\mathrm{s}$. The vertical dashed lines mark the points $k = k_0$ and $k = k_0\sqrt{\varepsilon_s/\varepsilon_0}$. The values of $B = 5$ T and $\mu_c = 115$ meV were used.

and $\langle\cdots\rangle$ denotes time average over one oscillation period. Here $Z = \sqrt{\mu/\varepsilon}$ is the impedance of the medium. Using Eqs. (A2) and (D2), the time-averaged Poynting vector can be cast as

$$\langle\mathbf{S}(\mathbf{r},t)\rangle = \frac{2\mu_0^2\omega_0^4}{Z}|\mathbb{G}(\mathbf{r},\mathbf{r}_0;\omega_0)\cdot\mathbf{d}_{\mathrm{ge}}|^2. \tag{D3}$$

In the limit $k_0|\mathbf{r}-\mathbf{r}_0| \gg 1$, the Green function $\mathbb{G}(\mathbf{r},\mathbf{r}_0;\omega_0)$ can be evaluated from Eq. (A5) using the stationary phase method (where the fast oscillating phase is given by $\boldsymbol{k}\cdot\boldsymbol{x} + ik_z^{(s)}|z|$). The obtained result is

$$\mathbb{G}(\mathbf{r},\mathbf{r}_0;\omega_0) \simeq \frac{-ik_n|z|}{2\pi r^2}e^{ik_n(r-\frac{z^2}{r})}\tilde{\mathbb{G}}\left(\frac{\boldsymbol{x}}{r}k_n, z, d; \omega_0\right), \tag{D4}$$

with $k_n = k_0$ for $z > 0$ and $k_n = k_0\sqrt{\varepsilon_s/\varepsilon_0}$ for $z < 0$. Using this result together with equations (A9), (A10), (D1), and (D3), one can put the total power emitted into the far field by the dipole as [36]

$$P_{\mathrm{rad}} = P_{\mathrm{rad}}^{\mathrm{up}} + P_{\mathrm{rad}}^{\mathrm{down}}, \tag{D5}$$

where $P_{\mathrm{rad}}^{\mathrm{up}}$ and $P_{\mathrm{rad}}^{\mathrm{down}}$ are the average powers emitted into the regions $z > 0$ and $z < 0$, respectively. Splitting each term into contributions from dipole components that are perpendicular and parallel to the XY plane, performing the integral over ϕ and changing the variable of integration θ according to $k = k_0\sin\theta$ for $P_{\mathrm{rad}}^{\mathrm{up}}$ and $k = k_0\sqrt{\varepsilon_s/\varepsilon_0}\sin\theta$ for $P_{\mathrm{rad}}^{\mathrm{down}}$, we can express the average powers as

$$\frac{P_{\mathrm{rad},\perp}^{\mathrm{up}}}{P_0} = \frac{1}{2} + \frac{3}{4}\int_0^{k_0} dk \frac{k^3}{k_0^3|k_z|}\{2\mathrm{Re}[e^{2ik_z d}r^{\mathrm{p,p}}] + |r^{\mathrm{p,p}}|^2 + |r^{\mathrm{s,p}}|^2\}, \tag{D6}$$

$$\frac{P_{\mathrm{rad},\parallel}^{\mathrm{up}}}{P_0} = \frac{1}{2} + \frac{3}{8}\int_0^{k_0} dk \frac{k}{k_0|k_z|}\left\{2\mathrm{Re}\left[e^{2ik_z d}\left(r^{\mathrm{s,s}} - \frac{|k_z|^2}{k_0^2}r^{\mathrm{p,p}}\right)\right] + |r^{\mathrm{s,s}}|^2 + \frac{|k_z|^2}{k_0^2}|r^{\mathrm{p,p}}|^2 + |r^{\mathrm{p,s}}|^2 + \frac{|k_z|^2}{k_0^2}|r^{\mathrm{s,p}}|^2\right\}, \tag{D7}$$

$$\frac{P_{\mathrm{rad},\perp}^{\mathrm{down}}}{P_0} = \frac{3}{4}\int_0^{k_0\sqrt{\varepsilon_s/\varepsilon_0}} dk \frac{k^3}{k_0^3|k_z|}e^{-2d\mathrm{Im}k_z}\frac{|k_z^s|}{|k_z|}\{|t^{\mathrm{p,p}}|^2 + |t^{\mathrm{s,p}}|^2\}, \tag{D8}$$

$$\frac{P_{\mathrm{rad},\parallel}^{\mathrm{down}}}{P_0} = \frac{3}{8}\int_0^{k_0\sqrt{\varepsilon_s/\varepsilon_0}} dk \frac{k}{k_0|k_z|}e^{-2d\mathrm{Im}k_z}\frac{|k_z^s|}{|k_z|}\left\{|t^{\mathrm{s,s}}|^2 + \frac{|k_z|^2}{k_0^2}|t^{\mathrm{p,p}}|^2 + |t^{\mathrm{p,s}}|^2 + \frac{|k_z|^2}{k_0^2}|t^{\mathrm{s,p}}|^2\right\}, \tag{D9}$$

where $P_0 = \omega_0^4 |\mathbf{d}_{ge}|^2/(3\pi\varepsilon_0 c^3) = \hbar\omega_0\Gamma_0$ is the total power emitted in free space. For the power emitted into the $z < 0$ region, there are two different contributions: (i) $\pi/2 < \theta < \arcsin(\sqrt{\varepsilon_s/\varepsilon_0})$, or $k_0 < k < k_0\sqrt{\varepsilon_s/\varepsilon_0}$, which is usually referred to as *forbidden light region* [36] and corresponds to an inverted total internal reflection process, in which a decaying wave that is emitted by the dipole is transmitted as a propagating wave once it reaches the interface (we refer to this contribution as $P_{\text{rad}}^{\text{down,f}}$); (ii) $\arcsin(\sqrt{\varepsilon_s/\varepsilon_0}) < \theta < \pi$, or $k < k_0$, which corresponds to the emission of propagating waves (we refer to this contribution as $P_{\text{rad}}^{\text{down,a}}$). By subtracting the power emitted via the radiative processes (P_{rad}) from the total dissipated power ($P_{\text{total}} = \hbar\omega_0\Gamma$), we obtain the power dissipated via nonradiative processes (P_{nonrad}). The contributions of the perpendicular and parallel components of the electric dipole to nonradiative power can be written in terms of absorption coefficients as

$$\frac{P_{\text{nonrad},\perp}}{P_0} = \frac{3}{4}\int_0^{+\infty} dk \frac{k^3 e^{-2d\text{Im}k_z}}{|k_z|k_0^3}\mathcal{A}_{\text{p}}, \tag{D10}$$

$$\frac{P_{\text{nonrad},\parallel}}{P_0} = \frac{3}{8}\int_0^{+\infty} dk \frac{k e^{-2d\text{Im}k_z}}{|k_z|k_0}\left(\mathcal{A}_{\text{s}} + \frac{|k_z|^2}{k_0^2}\mathcal{A}_{\text{p}}\right), \tag{D11}$$

where the absorption coefficients are given by

$$\mathcal{A}_{\text{p}} = \begin{cases} 1 - \left[|r^{\text{p,p}}|^2 + |r^{\text{s,p}}|^2 + \frac{|k_z^s|}{|k_z|}(|t^{\text{p,p}}|^2 + |t^{\text{s,p}}|^2)\right], & k < k_0, \\ 2\text{Im}[r^{\text{p,p}}] - \frac{|k_z^s|}{|k_z|}(|t^{\text{p,p}}|^2 + |t^{\text{s,p}}|^2), & k_0 < k < k_0\sqrt{\varepsilon_s/\varepsilon_0}, \\ 2\text{Im}[r^{\text{p,p}}], & k_0\sqrt{\varepsilon_s/\varepsilon_0} < k, \end{cases} \tag{D12}$$

and $\mathcal{A}_{\text{s}}$ is obtained from Eq. (D12) by swapping $s \leftrightarrow p$.

Note that for $k > k_0\sqrt{\varepsilon_s/\varepsilon_0}$ the expressions for the nonradiative emitted power, Eqs. (D10) and (D11), coincide with the expressions for the total SE rate, Eqs. (1) and (2). Hence, we can interpret the integration region $k > k_0\sqrt{\varepsilon_s/\varepsilon_0}$ in Eqs. (1) and (2) as being a contribution to the SE rate exclusively due to nonradiative processes. The region $k < k_0\sqrt{\varepsilon_s/\varepsilon_0}$ also contributes to the nonradiative decay, as can be seen in Fig. 5, where the integrands of Eqs. (D10) and (D11) as a function of k are plotted. This is only expected as propagating waves emitted by the dipole can also be absorbed and dissipated by the graphene layer. It should be mentioned, however, that the contribution of wave vectors $k < k_0\sqrt{\varepsilon_s/\varepsilon_0}$ to the nonradiative SE decay is negligible when compared to the contribution coming from $k > k_0\sqrt{\varepsilon_s/\varepsilon_0}$ (see Fig. 5). Therefore, the nonradiative decay due to LSW can be well approximated by Eq. (9). In the same way, we can approximate the contribution to the SE rate from $k < k_0\sqrt{\varepsilon_s/\varepsilon_0}$ in Eqs. (1) and (2) as being exclusively owing to radiative processes. As such, we can approximate $P_{\text{rad},\perp}^{\text{down,f}}$ (TIR modes) by Eq. (8) and $P_{\text{rad},\perp}^{\text{down,a}} + P_{\text{rad},\perp}^{\text{up}}$ (propagating modes) by Eq. (7). Approximations (7) and (8) were tested numerically against the exact results and the differences were found to be negligible.

Finally, we notice that the power emitted by the quantum emitter that is absorbed by graphene due to Joule heating can be written as

$$P_{\text{g}} = 2\mu^2\omega_0^4\,\text{Re}\int \frac{d^2\boldsymbol{k}}{(2\pi)^2}\mathbf{d}_{\text{ge}}^* \cdot \tilde{\mathbb{G}}^{\dagger}(\boldsymbol{k},0,0;\omega_0)\cdot \times \boldsymbol{\sigma}(\boldsymbol{k},\omega_0)\cdot\tilde{\mathbb{G}}(\boldsymbol{k},0,0;\omega_0)\cdot\mathbf{d}_{ge}. \tag{D13}$$

In the case when $\text{Im}[\varepsilon_s] = 0$, nonradiative decay is exclusively due to graphene and it is possible to show that the power absorbed by graphene can be written as Eqs. (D10) and (D11), with absorption coefficients given by Eq. (D12).

[1] E. M. Purcell, Phys. Rev. **69**, 37 (1946).
[2] V. V. Klimov and V. S. Letokhov, Chem. Phys. Lett. **301**, 441 (1999).
[3] M. S. Tomas, Phys. Rev. A **63**, 053811 (2001).
[4] V. V. Klimov, M. Ducloy, and V. S. Letokhov, Sov. J. Quantum Electron. **31**, 569 (2001).
[5] L. A. Blanco and F. J. García de Abajo, Phys. Rev. B **69**, 205414 (2004).
[6] M. Thomas, J.-J. Greffet, R. Carminati, and J. R. Arias-Gonzalez, Appl. Phys. Lett. **85**, 3863 (2004).
[7] R. Carminati, J.-J. Greffet, C. Henkel, and J. M. Vigoureaux, Opt. Commun. **261**, 368 (2006).
[8] F. S. S. Rosa, T. N. C. Mendes, A. Tenório, and C. Farina, Phys. Rev. A **78**, 012105 (2008).
[9] S.-A. Biehs and J.-J. Greffet, Phys. Rev. A **84**, 052902 (2011).
[10] D. T. Alves, C. Farina, and A. C. Tort, Phys. Rev. A **61**, 034102 (2000).
[11] Y. V. Vladimirova, V. V. Klimov, V. M. Pastukhov, and V. N. Zadkov, Phys. Rev. A **85**, 053408 (2012).
[12] E. Betzig and R. J. Chichester, Science **262**, 1422 (1993).
[13] R. X. Bian, R. C. Dunn, X. S. Xie, and P. T. Leung, Phys. Rev. Lett. **75**, 4772 (1995).
[14] E. J. Sanchez, L. Novotny, and X. S. Xie, Phys. Rev. Lett. **82**, 4014 (1999).
[15] J.-J. Greffet, Science **308**, 1561 (2005).
[16] P. Muhlschlegel, H. J. Eisler, O. J. F. Martin, B. Hecht, and D. W. Pohl, Science **308**, 1607 (2005).
[17] V. V. Klimov, Opt. Commun. **211**, 183 (2002).
[18] C. L. Cortes, W. Newman, S. Molesky, and Z. Jacob, J. Opt. **14**, 063001 (2012).
[19] Z. Jacob, I. I. Smolyaninov, and E. E. Narimanov, Appl. Phys. Lett. **100**, 181105 (2012).
[20] W. J. M. Kort-Kamp, F. S. S. Rosa, F. A. Pinheiro, and C. Farina, Phys. Rev. A **87**, 023837 (2013).

[21] J. B. Jackson and N. J. Halas, Proc. Natl. Acad. Sci. USA **101**, 17930 (2004).

[22] H. Wei, F. Hao, Y. Huang, W. Wang, P. Nordlander, and H. Xu, Nano Lett. **8**, 2497 (2008).

[23] J. F. Li *et al.*, Nature (London) **464**, 392 (2010).

[24] G. M. Akselrod, C. Argyropoulos, T. B. Hoang, C. Ciracì, C. Fang, J. Huang, D. R. Smith, and M. H. Mikkelsen, Nat. Photonics **8**, 835 (2014).

[25] A. H. Castro Neto, F. Guinea, N. M. R. Peres, A. K. Geim, and K. S. Novoselov, Rev. Mod. Phys. **81**, 109 (2009).

[26] N. M. R. Peres, Rev. Mod. Phys. **82**, 2673 (2010).

[27] A. N. Grigorenko, M. Polini, and K. S. Novoselov, Nat. Photonics **6**, 749 (2012).

[28] Q. Bao and K. P. Loh, ACS Nano **6**, 3677 (2012).

[29] Y. V. Bludov, A. Ferreira, N. M. R. Peres, and M. I. Vasilevskiy, Int. J. Mod. Phys. B **27**, 1341001 (2013).

[30] F. J. García de Abajo, ACS Photonics **1**, 135 (2014).

[31] F. H. L. Koppens, D. E. Chang, and F. García de Abajo, Nano Lett. **11**, 3370 (2011).

[32] L. Gaudreau, K. J. Tielrooij, G. E. D. K. Prawiroatmodjo, J. Osmond, F. J. García de Abajo, and F. H. L. Koppens, Nano Lett. **13**, 2030 (2013).

[33] G. W. Hanson, E. Forati, W. Linz, and A. B. Yakovlev, Phys. Rev. B **86**, 235440 (2012).

[34] P. A. Huidobro, A. Y. Nikitin, C. González-Ballestero, L. Martín-Moreno, and F. J. García-Vidal, Phys. Rev. B **85**, 155438 (2012).

[35] K. J. Tielrooij *et al.*, Nat. Phys. **11**, 281 (2015).

[36] L. Novotny and B. Hecht, *Principles of Nano-Optics* (Cambridge University Press, Cambridge, UK, 2006).

[37] S. Haroche, *Cavity Quantum Electrodynamics* in *Fundamental Systems in Quantum Optics*, edited by J. Dalibard, J. M. Raimond, and J. Zinn Justin, Proceedings of the Les Houches Summer School of Theoretical Physics, LIII (North Holland, Amsterdam, 1992).

[38] W. J. M. Kort-Kamp, Ph.D. thesis, Universidade Federal do Rio de Janeiro, 2015.

[39] W.-K. Tse and A. H. MacDonald, Phys. Rev. B **84**, 205327 (2011).

[40] T. Cysne, W. J. M. Kort-Kamp, D. Oliver, F. A. Pinheiro, F. S. S. Rosa, and C. Farina, Phys. Rev. A **90**, 052511 (2014).

[41] G. W. Ford and W. H. Weber, Phys. Rep. **113**, 195 (1984).

[42] A. Ferreira, N. M. R. Peres, and A. H. Castro Neto, Phys. Rev. B **85**, 205426 (2012).

[43] G. Gómez-Santos and T. Stauber, Phys. Rev. B **84**, 165438 (2011).

[44] V. P. Gusynin and S. G. Sharapov, Phys. Rev. B **73**, 245411 (2006).

[45] V. P. Gusynin, S. G. Sharapov, and P. Cabotte, J. Phys. Condens. Matter **19**, 026222 (2007).

[46] M. O. Goerbig, Rev. Mod. Phys. **83**, 1193 (2011).

[47] R. G. Hulet, E. S. Hilfer, and D. Kleppner, Phys. Rev. Lett. **55**, 2137 (1985).

[48] L. Ju *et al.*, Nat. Nanotechnol. **6**, 630 (2011).

[49] I. Crasee, M. Orlita, M. Potemnski, A. L. Walter, M. Ostler, Th. Seyller, I. Gaponenko, J. Chen, and A. B. Kuzmenko, Nano. Lett. **12**, 2470 (2012).

[50] F. Guinea, M. I. Katsnelson, and A. K. Geim, Nat. Phys. **6**, 30 (2009).

[51] N. Levy, S. A. Burke, K. L. Meaker, M. Panlasigui, A. Zettl, F. Guinea, A. H. Castro Neto, and M. F. Crommie, Science **329**, 544 (2010).

[52] Since TIR waves ($k_0 < k \leqslant \sqrt{\varepsilon_s/\varepsilon_0}k_0$) propagate in the $z < 0$ region, a photon may be detected in the substrate. Hence, we are considering these waves as part of the radiative process of SE. If instead of a semi-infinite medium, the substrate is a finite slab in vacuum, these waves will be transmitted to the other side of the slab as evanescent waves and will not contribute to the radiation field. These modes will, however, be able to excite waveguide modes in the slab.

[53] One could think that there exists a lossless surface wave [e.g., surface phonon polariton (SPhP)] contribution coming from the SiC substrate. However, for the frequency considered, we have an essentially real and positive permittivity $[\varepsilon_s(\omega_0)/\varepsilon_0 \simeq 10 + 0.0006i]$, so no SPhP is supported.

[54] J. R. Lakowicz, Anal. Biochem. **337**, 171 (2005).

[55] W. L. Barnes, J. Mod. Opt. **45**, 661 (1998).

[56] It must be noted that the conductivity that enters the boundary conditions is a one-particle irreducible quantity (with respect to the EM propagator), as solving the Maxwell's equations automatically resumes bubble diagrams, including screening effects.

[57] T. Low, R. Roldán, H. Wang, F. Xia, P. Avouris, L. M. Moreno, and F. Guinea, Phys. Rev. Lett. **113**, 106802 (2014).